Dual-Band Metal Frame Blockage Reduction for 5G mm-Wave Arrays in Mobile Phones

Rodriguez-Cano, Rocio; Zhao, Kun; Zhang, Shuai; Pedersen, Gert F.

Published in:
16th European Conference on Antennas and Propagation, EuCAP 2022

DOI (link to publication from Publisher):
10.23919/EuCAP53622.2022.9769010

Creative Commons License
Unspecified

Publication date:
2022

Document Version
Accepted author manuscript, peer reviewed version

Dual-Band Metal Frame Blockage Reduction for 5G mm-Wave Arrays in Mobile Phones

Rocio Rodriguez-Cano, Kun Zhao, Shuai Zhang, Gert F. Pedersen
APMS section, Department of Electronic Systems, Aalborg University, Aalborg, Denmark
{*rrc, kz, sz, gfp*}*@es.aau.dk*

***Abstract*—This paper proposes a solution that allows reducing the obstruction from the mobile phone frame to electromagnetic waves in two bands of the mm-wave spectrum. This response is obtained by etching longitudinal corrugations of two different lengths in the metal frame. The corrugations are inspired on the hard surfaces principle, which supports the propagation of electromagnetic waves on metal. The proposed structure is matched to a 50-Ohm source in the following bands: 25.4-27.7 GHz, 28.7-29.9 GHz, and 36.4-40.3 GHz. The realized gain of the mm-wave array with the corrugated frame is higher than the one of the array in free space in the majority of the operating bandwidth. The proposed solution can increase the gain of the array with a normal frame up to 10 dB.**

***Index Terms*—antenna array, 5G, mm-wave, frame, blockage, hard surface, dual-band.**

I. Introduction

The limited space left in mobile terminals has motivated the co-existence of sub-7 GHz frame antennas [1], [2] and the new mm-wave arrays in the 5^{th} generation of mobile communication (5G) [3]–[9]. Bezels are an inherent part of mobile terminals that hold the display and back cover together. The majority of bezels are made of metal, which does not allow the propagation of electromagnetic waves through them. The tear-downs from the latest 5G mm-wave-enabled phones show that mm-wave modules can be located at the long edges of the phone, right in front of the metallic bezel. In order to allow the propagation of the mm-wave radiation, windows are made on the bezel, filled with some dielectric material [10].

Etching large windows on the bezel [6], [10] weakens the robustness of the frame, modifies the current distribution, and affects the aesthetic quality. Only a few other solutions can be found in the literature. In [5] two tilted layers of strips are placed at both sides of the frame to couple the energy impinging on the frame and adding it in-phase in the far-field. Several slots are etched on the frame in [7], which are fed by the energy radiated by the mm-wave array. This method is improved in [11] to cover a wider frequency band, with additional slots on the frame. In [8] a chain-slot is also etched on the frame. In [12], hard surface inspired corrugations were proposed by the authors to allow the propagation of mm-wave radiation in one frequency band. A hard surface is formed by loading a conducting surface with longitudinal corrugations filled with dielectric, or by placing longitudinal metal strips on a thin dielectric layer [13].

Apart from the bands in the sub-7 GHz spectrum, 5G includes a new frequency range (FR2) in the mm-wave spectrum. In particular, several bands have been defined between 24.25 GHz and 52.6 GHz [14]. In this paper, we address the necessity of covering multiple bands in the mm-wave spectrum, by improving our previous design to operate at several frequency bands.

II. Operating principle

The design is inspired by the operational mechanism of hard surfaces, which support the propagation of electromagnetic waves in the metallic surface thanks to the etching of longitudinal corrugations, filled with a dielectric material. The operating principle is represented in Fig. 1. These corrugations make the frame transparent to electromagnetic waves at a certain frequency and allow the energy to pass through. The hard boundary condition provides strong radiation fields along the surface [13].

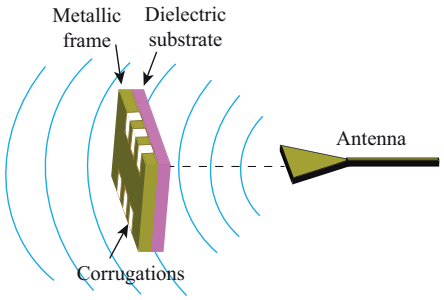

Fig. 1. Operating principle of the hard surface inspired frame [15].

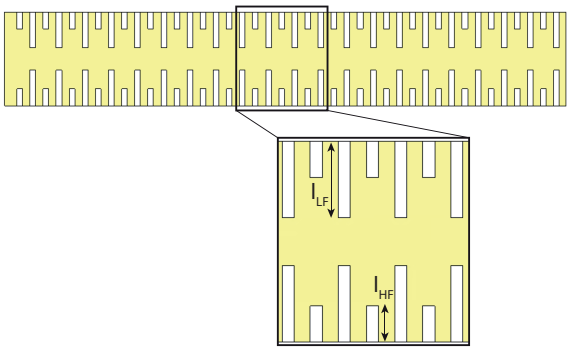

Fig. 2. Dual-band metallic frame model with corrugations.

In this dual-band design, corrugations of two different sizes (l_{LF}, l_{HF}) are etched on the metallic frame, as Fig. 2 shows.

The shorter set of corrugations is located in the middle of two long ones.

The corrugations length controls the operational band, and their value should be comprised between $\lambda_g/4$ and $\lambda_g/2$. As the length depends on the guided wavelength, substrates with higher permittivity values meet the requirement with shorter lengths, which makes this solution less noticeable to the human eye and improves the robustness of the frame.

III. Scattering Investigation of the Metal Frame

To evaluate the performance of the frame alone, without the influence of the antenna array, and with plane wave illumination, the Radar Cross Section (RCS) has been obtained in Fig. 3. The RCS measures the scattering properties of the frame with plane wave illumination. For that reason, low values of RCS are desired in the targeted frequency bands.

When the frame is illuminated by a plane wave, the lengths of the two different corrugations can be adjusted independently to achieve a dual-band response. Fig. 3a shows that the longer corrugation (l_{LF}) controls the resonance in the lower band, with longer values of l_{LF} shifting downwards the resonance.

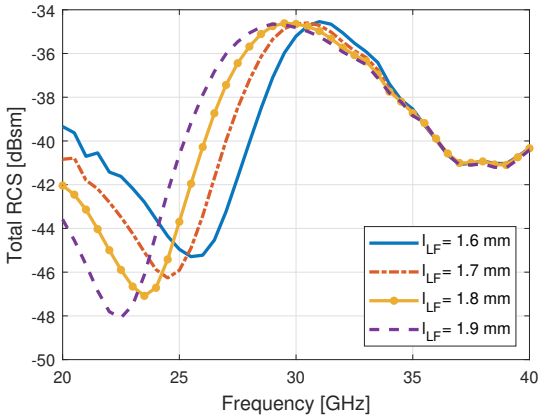

(a)

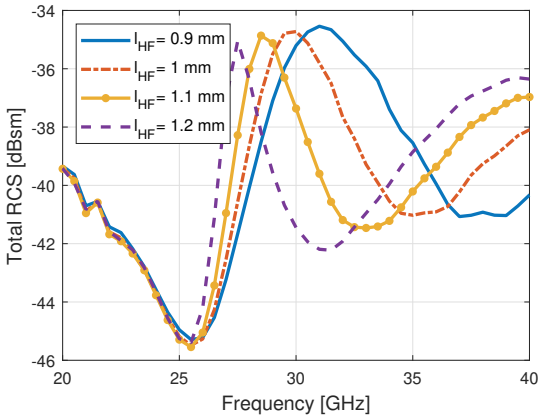

(b)

Fig. 3. Total RCS of the corrugated frame illuminated by a plane wave. (a) Longer corrugation length sweep (l_{LF}). (b) Shorter corrugation length sweep (l_{HF}).

On the other hand, Fig. 3b represents the effect of changing the length of the corrugation controlling the higher band l_{HF} of the design. When longer lengths are chosen, the resonance in the higher band also shifts down in frequency. The lowest RCS value in the second band is provided by $l_{HF} = 1.2$ mm at 31 GHz.

Once that the parameter behavior has been analyzed, the final design operating in the desired frequency bands is presented in the next section.

IV. Antenna Integration Performance

The proposed design is represented in Fig. 4a. The substrates of the frame and antenna array have been hidden for a better comprehension of the structure. The antenna printed circuit board (PCB) is separated 1 mm from the substrate of the frame. Rogers RO3006 has been chosen for both substrates, with $\epsilon_r = 6.15$ and $tan\delta = 0.002$. The thickness of the PCB is 0.13 mm and the frame substrate is 0.64 mm. For the final design, l_{LF} has a value of 1.45 mm and l_{HF}, 1.2 mm; while the widths are 0.3 mm and 0.2 mm, respectively. The mm-wave array is composed of three dipole antennas with a strip placed in front of them to provide a second resonance at higher frequency (Fig. 4b). In particular, the total length of the dipole is 3.73 mm and the short strip is 2 mm. The mm-wave array is similar to the one in [11], but adapted to a higher permittivity substrate.

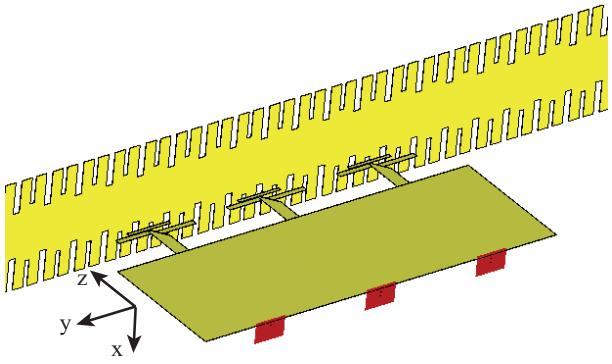

(a)

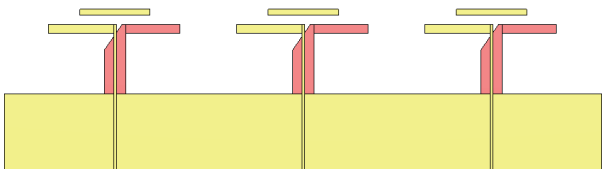

(b)

Fig. 4. (a) Full model of the mm-wave antenna array with the dual-band hard surface-inspired frame. The substrates of the frame and antenna have been hidden to show the full structure. (b) Millimeter-wave dipole antenna array.

The placement of the hard-surface inspired corrugated frame in front of the mm-wave antenna array, produces some coupling between the structures, and it is no longer possible to control the two resonances independently, as the realized gain in Fig. 5 shows. By increasing the value of the high frequency

corrugation, the first resonance shifts downwards in frequency, while the second resonance mainly increases the realized gain value. It is also possible to see that for the same value of l_{HF}, the presence of the antenna shifts both resonances upwards in frequency.

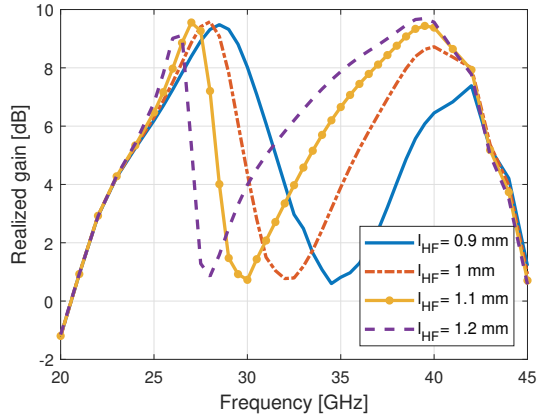

Fig. 5. Realized gain in the endfire direction as a function of the frequency for different lengths of the high frequency notch.

The reflection coefficient of the three ports of the mm-wave antenna is plotted in Fig. 6. The antenna meets the -10 dB matching criterion in the next bands: $25.4-27.7$ GHz, $28.7-29.9$ GHz and $36.4-40.3$ GHz.

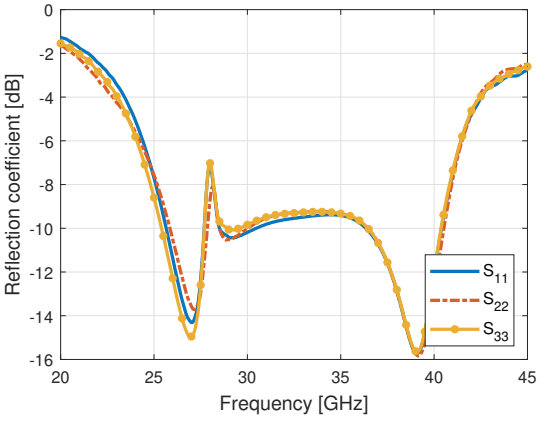

Fig. 6. Reflection coefficient of the proposed design.

The radiation patterns of the proposed design, at two different frequencies, are plotted in Fig. 7 (see coordinate system in Fig. 4a). The first one corresponds to a frequency of 27.8 GHz, reaching 8.9 dBi and front-to-back ratio (FTBR) of 14 dB. The pattern in Fig. 7b, corresponds to 39 GHz, with a peak gain of 9.44 dBi and FTBR of 12.4 dB.

Fig. 8 shows the realized gain comparison between the free space array, the array with a normal frame and the hard surface-inspired solution. The proposed solution improves the gain compared to the array in free space in the operating bands. It presents a substantial improvement compared with

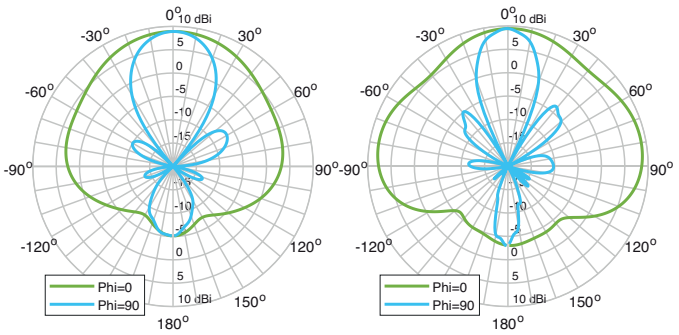

Fig. 7. Realized gain radiation patterns. (a) f= 27.8 GHz. (b) f= 39 GHz.

the normal frame solution, in which the majority of the radiation is not in the endfire direction.

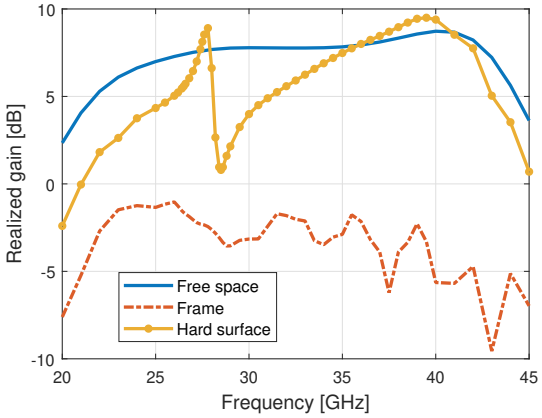

Fig. 8. Realized gain comparison of the array in free space, with a normal frame and with the hard surface inspired solution in the endfire direction.

V. Conclusion

The manuscript proposes a dual-band method to reduce the metal frame blockage in handsets to the electromagnetic radiation from the mm-wave modules.

The mm-wave array chosen to verify the theory is composed of three dipole elements, but other antenna topologies and phone factors can be employed. The realized gain results show a 5 to 10 dB gain increment of the proposed structure compared to the normal metal frame. The array with corrugated frame can even improve the free space gain in parts of the operating bandwidth. This makes the proposed structure an attractive candidate for the implementation of mm-wave endfire arrays into mobile terminals.

Acknowledgment

This work was partially supported by the Innovations-Fonden project of Reconfigurable Arrays for Next Generation Efficiency (RANGE), and by research grant (41389) from VILLUM FONDEN.

REFERENCES

[1] Y. Liu, W. Cui, Y. Jia, and A. Ren, "Hepta-band metal-frame antenna for LTE/WWAN full-screen smartphone," *IEEE Antennas and Wireless Propagation Letters*, vol. 19, no. 7, pp. 1241–1245, 2020.

[2] H. Chen and A. Zhao, "LTE antenna design for mobile phone with metal frame," *IEEE Antennas and Wireless Propagation Letters*, vol. 15, pp. 1462–1465, 2016.

[3] J. Kurvinen, R. M. Moreno, A. Lehtovuori, J. Ala-Laurinaho, J. Ilvonen, A. Khripkov, and V. Viikari, "Low-band LTE antenna integrated into mm-wave handset antenna," in *2021 15th European Conference on Antennas and Propagation (EuCAP)*, 2021, pp. 1–3.

[4] H. Li, Y. Cheng, L. Mei, and L. Guo, "Frame integrated wideband dual-polarized arrays for mm-wave/sub 6-Ghz mobile handsets and its user effects," *IEEE Transactions on Vehicular Technology*, vol. 69, no. 12, pp. 14 330–14 340, 2020.

[5] R. Rodriguez-Cano, S. Zhang, K. Zhao, and G. F. Pedersen, "Reduction of main beam-blockage in an integrated 5G array with a metal-frame antenna," *IEEE Trans. Antennas Propag.*, vol. 67, no. 5, pp. 3161–3170, May 2019.

[6] J. Kurvinen, H. Kähkönen, A. Lehtovuori, J. Ala-Laurinaho, and V. Viikari, "Co-designed mm-wave and LTE handset antennas," *IEEE Trans. Antennas Propag.*, vol. 67, no. 3, pp. 1545–1553, March 2019.

[7] R. Rodriguez-Cano, S. Zhang, K. Zhao, and G. F. Pedersen, "mm-wave beam-steerable endfire array embedded in a slotted metal-frame LTE antenna," *IEEE Transactions on Antennas and Propagation*, vol. 68, no. 5, pp. 3685–3694, 2020.

[8] R. M. Moreno, J. Kurvinen, J. Ala-Laurinaho, A. Khripkov, J. Ilvonen, J. van Wonterghem, and V. Viikari, "Dual-polarized mm-wave endfire chain-slot antenna for mobile devices," *IEEE Transactions on Antennas and Propagation*, vol. 69, no. 1, pp. 25–34, 2020.

[9] Z. Zhu, H.-C. Huang, Y. Wang, X. Jian, and R. Ma, "Embedded 5G wideband dual-polarized mm-wave antennas in non-mm-wave antennas integrating a package (AiAiP) for a metal-framed cell phone," in *2020 14th European Conference on Antennas and Propagation (EuCAP)*, 2020, pp. 1–5.

[10] Ifixit. (2020) iPhone 12 and 12 Pro teardown. [Online]. Available: www.ifixit.com/Teardown/iPhone+12+and+12+Pro+Teardown/137669

[11] R. Rodriguez-Cano, K. Zhao, S. Zhang, and G. F. Pedersen, "Wideband reduction of the metal-frame blockage to mm-wave antennas," in *2021 15th European Conference on Antennas and Propagation (EuCAP)*, 2021, pp. 1–4.

[12] R. Rodriguez-Cano, K. Zhao, S. Zhang, and G. F. Pedersen, "Handset frame blockage reduction of 5G mm-wave phased arrays using hard surface inspired structure," *IEEE Transactions on Vehicular Technology*, vol. 69, no. 8, pp. 8132–8139, 2020.

[13] P.-S. Kildal, "Artificially soft and hard surfaces in electromagnetics," *IEEE Transactions on Antennas and Propagation*, vol. 38, no. 10, pp. 1537–1544, 1990.

[14] "User Equipment (UE) radio transmission and reception; Part 2: Range 2 Standalone (3GPP TS 38.101-2 version 16.4.0 Release 16)," 3rd Generation Partnership Project (3GPP), Technical Specification (TS) 38.101-2, 07 2020, version 16.4.0.

[15] R. Rodriguez-Cano, "Integration of mm-wave antenna systems in 5g mobile terminals," Ph.D. dissertation, Aalborg University, 2020.